

Robust and Optimal Control of Magnetic Microparticles Inside Fluidic Channels with Time-varying Flow Rates

Regular Paper

Islam S.M. Khalil^{1*}, Hazem Abass¹, Mostafa Shoukry¹, Anke Klingner¹, Rasha M. El-Nashar², Mohamed Serry³ and Sarthak Misra⁴

¹ German University in Cairo, New Cairo, Egypt

² Cairo University, Cairo, Egypt

³ American University in Cairo, New Cairo, Egypt

⁴ University of Twente, Enschede, The Netherlands

*Corresponding author(s) E-mail: islam.shoukry@guc.edu.eg

Received 31 December 2015; Accepted 07 April 2016

DOI: 10.5772/63517

© 2016 Author(s). Licensee InTech. This is an open access article distributed under the terms of the Creative Commons Attribution License (<http://creativecommons.org/licenses/by/3.0>), which permits unrestricted use, distribution, and reproduction in any medium, provided the original work is properly cited.

Abstract

Targeted therapy using magnetic microparticles and nanoparticles has the potential to mitigate the negative side-effects associated with conventional medical treatment. Major technological challenges still need to be addressed in order to translate these particles into *in vivo* applications. For example, magnetic particles need to be navigated controllably in vessels against flowing streams of body fluid. This paper describes the motion control of paramagnetic microparticles in the flowing streams of fluidic channels with time-varying flow rates (maximum flow is 35 ml.hr⁻¹). This control is designed using a magnetic-based proportional-derivative (PD) control system to compensate for the time-varying flow inside the channels (with width and depth of 2 mm and 1.5 mm, respectively). First, we achieve point-to-point motion control against and along flow rates of 4 ml.hr⁻¹, 6 ml.hr⁻¹, 17 ml.hr⁻¹, and 35 ml.hr⁻¹. The average speeds of single microparticle (with average diameter of 100 μm) against flow rates of 6 ml.hr⁻¹ and 30 ml.hr⁻¹ are calculated to be 45 μm.s⁻¹ and 15 μm.s⁻¹, respectively. Second, we implement PD control with disturbance estimation and compensation. This

control decreases the steady-state error by 50%, 70%, 73%, and 78% at flow rates of 4 ml.hr⁻¹, 6 ml.hr⁻¹, 17 ml.hr⁻¹, and 35 ml.hr⁻¹, respectively. Finally, we consider the problem of finding the optimal path (minimal kinetic energy) between two points using calculus of variation, against the mentioned flow rates. Not only do we find that an optimal path between two collinear points with the direction of maximum flow (middle of the fluidic channel) decreases the rise time of the microparticles, but we also decrease the input current that is supplied to the electromagnetic coils by minimizing the kinetic energy of the microparticles, compared to a PD control with disturbance compensation.

Keywords Time-varying Flow, Magnetic, Microfluidic Channel, Microparticles, Disturbance, Optimal Control

1. Introduction

Recently, magnetic micro and nanoparticles have attracted much interest in nanomedicine and nanotechnology [1, 2]. Their miniature size allows them to access deep-seated

regions within the human body and execute targeted therapy and diverse biomedical applications [3-9]. Many researchers have proposed the utilization of biodegradable magnetic nanocapsules, nanoparticles, and microparticles (magnetic drug carriers) in drug delivery applications [10-14]. These carriers can be injected into the human body through the circulatory system, and external magnetic fields are applied to concentrate these carriers at a specific diseased cell. The miniature size of these carriers makes their motion control and positioning a challenge in the presence of flowing streams of a fluid; these problems are most likely to occur in biomedical applications and targeted therapy.

A few research groups have proposed a variety of self-driven [15-17] and magnetically-driven [18] mechanisms to overcome the flowing streams inside fluidic channels. Open-loop control of self-propelled microjets has been achieved inside fluidic channels against the flowing streams of hydrogen peroxide solution [15]. The control accuracy of these microjets has been improved using closed-loop control with microscopic image guidance. This control has enabled propulsion of the microjets along and against the flowing streams of the hydrogen peroxide solution [19]. Although these microjets can overcome the flowing streams of the solution and achieve non-trivial tasks, their locomotion mechanism does not allow them to be used in biomedical applications, because of the toxicity. No research has yet addressed the optimal path that allows the microjet to reach a reference position in minimal time or with minimal control effort. Positioning of ferromagnetic nanoparticles inside rats was achieved by Nacev *et al.* [20] by directing external magnetic fields towards a desired position without feedback. Belharet *et al.* presented a method for predictive control of magnetic microrobots in a microfluidic arterial bifurcations using fluids with different viscosities [18]. Minimal input control of paramagnetic microparticles in three-dimensional (3D) space has been achieved using an electromagnetic system with closed configuration [21]. This optimal control might increase the availability of electromagnetic coils during the positioning of the microparticles in 3D space, as the input current to the electromagnetic coils is decreased. However, magnetic control has been achieved in a stationary fluid without flow. In this study, we achieve the following:

- Modelling of the motion of paramagnetic microparticles in flowing streams inside fluidic channels;
- Development of a robust closed-loop motion control system that allows for the positioning of the microparticles within the vicinity of a reference position in the presence of time-varying flow;
- Finding the optimal path that enables controlled motion against the flow towards the reference position with minimal kinetic energy.

We analyse the motion of the microparticles in a low-Reynolds-number regime, and develop a model for their motion in a fluid with a time-varying flow rate (Fig. 1). This model is used in the design of a robust motion control

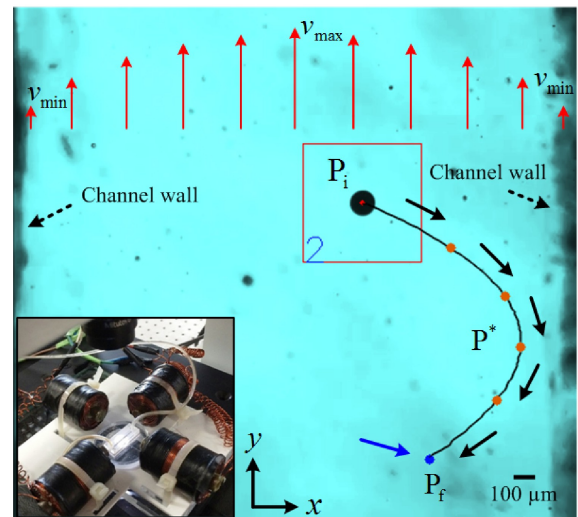


Figure 1. A controlled paramagnetic microparticle moving along an optimal trajectory against time-varying flow inside a fluidic channel. Maximum and minimum flows (v_{\max} and v_{\min}) are observed at the middle and close to the walls of the channel (indicated using the red arrows). The control system provides an optimal quadratic path that allows the microparticle to avoid relatively large drag force (in the middle of the channel), and hence to move towards the reference position with lower magnetic field gradient. The controlled magnetic field gradients are generated using the electromagnetic system shown in the bottom-left corner. The black line and small orange circles indicate the optimal path (P^*) and the waypoints along the path, respectively. The initial and final positions of the microparticle are indicated using P_i and P_f , respectively. The blue and black arrows represent the reference position and the direction of the microparticle, respectively. The black dashed arrows indicate the walls of the channel.

system based on disturbance force estimation and compensation [22]. In addition, we find the path that allows the microparticles to move towards a reference position with minimal energy to decrease the kinetic energy of the controlled microparticles.

The remainder of this paper is organized as follows: Section 2 provides modelling of the motion of microparticles inside fluidic channels [23] and a comparison between the model and the experimental results. The designs of robust and optimal motion control systems are included in Section 3 using a disturbance observer technique and the calculus of variation theory, respectively. Section 3 also provides motion-control experimental results using a magnetic system with orthogonal electromagnetic configuration and under microscopic guidance. Discussions pertaining to the magnetic-based motion control of microparticles and the challenges that have to be overcome to translate them into biomedical applications are provided in Section 4. Finally, Section 5 concludes and provides directions for future work.

2. Modelling and Characterization of Microparticles Inside Channels

The motion of a magnetic microparticle under the influence of a magnetic field ($\mathbf{B}(\mathbf{P})$) and in a fluid (with volume V) with time-varying flow rate ($Q(t) = \frac{dV}{dt}$) is governed by

$$\mathbf{F}_B(\mathbf{P}) + \mathbf{F}_Q(\mathbf{P}) + \mathbf{F}_d(\dot{\mathbf{P}}) = 0, \quad (1)$$

where $\mathbf{F}_B(\mathbf{P}) \in \mathbb{R}^{3 \times 1}$ is the magnetic force at point $(\mathbf{P} \in \mathbb{R}^{3 \times 1})$, $\mathbf{F}_Q(\mathbf{P}) \in \mathbb{R}^{3 \times 1}$ is the force due to time-varying flow rate, and $\mathbf{F}_d(\dot{\mathbf{P}}) \in \mathbb{R}^{3 \times 1}$ is the drag force on the microparticle. The magnetic force exerted on the microparticle is generated using an orthogonal configuration of electromagnetic coils (Fig. 2) and is given by [24]

$$\mathbf{F}_B(\mathbf{P}) = (\mathbf{m} \cdot \nabla) \mathbf{B}(\mathbf{P}) = (\mathbf{m} \cdot \nabla) \tilde{\mathbf{B}}(\mathbf{P}) \mathbf{I} = \Lambda(\mathbf{m}, \mathbf{P}) \mathbf{I}, \quad (2)$$

where $\mathbf{m} \in \mathbb{R}^{3 \times 1}$ and $\mathbf{B}(\mathbf{P}) \in \mathbb{R}^{3 \times 1}$ are the magnetic dipole moment of the microparticle and the induced magnetic field, respectively [10, 25]. $\tilde{\mathbf{B}}(\mathbf{P}) \in \mathbb{R}^{3 \times 4}$ and $\mathbf{I} \in \mathbb{R}^{4 \times 1}$ are the magnetic field-current map and the input current to the four electromagnetic coils, respectively. Furthermore, $\Lambda(\mathbf{m}, \mathbf{P}) \in \mathbb{R}^{4 \times 3}$ is the magnetic force-current map of the magnetic configuration. The largest microparticle we use in this study is less than 100 μm in diameter (PLAParticles-M-redF-plain from Micromod Partikeltechnologie GmbH, Rostock-Warnemuende, Germany), and the maximum magnetic field gradient exerted on its dipole moment is 221 $\text{mT} \cdot \text{mm}^{-1}$. The Reynolds number $\left(R_e = \frac{\rho Q}{h\eta}\right)$ is calculated to be less than 0.1 for the density (ρ) of the fluid (900 $\text{kg} \cdot \text{m}^{-3}$ for oil [28]), maximum flow rate 35 $\text{ml} \cdot \text{hr}^{-1}$, viscosity (η) of the fluid (50 $\text{mPa} \cdot \text{s}$ for oil [2]), and characteristic channel side-length (h) of 1.5 mm. Therefore, we can assume laminar flow condition, and the fluid velocity vector $\mathbf{v}(\mathbf{P})$ is calculated as follows [26]:

$$\mathbf{v}(\mathbf{P}) = -\frac{2Q}{A} \left(1 - \frac{4x^2}{w^2}\right) \hat{\mathbf{y}}, \quad (3)$$

where x is the x -component of the position vector (\mathbf{P}) from the centre of the channel. The flow rate (Q) is applied along a negative $\hat{\mathbf{y}}$ direction, where $\hat{\mathbf{y}}$ is a unit-vector opposite to the direction of flow, as shown in Fig. 2. Furthermore, A is the cross-sectional area of the channel. In our experimental set-up, the cross-sectional area is rectangular, with height (h) and width (w) of 1.5 mm and 2 mm, respectively. This cross-section allows us to induce flow rates approximately similar to mouse carotid flow rates, which average between 14.4 $\text{ml} \cdot \text{hr}^{-1}$ and 42 $\text{ml} \cdot \text{hr}^{-1}$ [20]. A time-varying flow rate results in a force due to acceleration of the fluid that is given by

$$\mathbf{F}_Q(\mathbf{P}) = M_p \frac{\rho_f}{\rho_p} \frac{d\mathbf{v}(\mathbf{P})}{dt} = -\frac{2M_p \rho_f \dot{Q}}{\rho_p A} \left(1 - \frac{4x^2}{w^2}\right) \hat{\mathbf{y}}. \quad (4)$$

In (4), M_p and \dot{Q} are the mass of the magnetic microparticle and time-derivative of the flow rate $\left(\dot{Q} = \frac{dQ}{dt}\right)$, respectively. ρ_f and ρ_p are the density of the fluid and the microparticle,

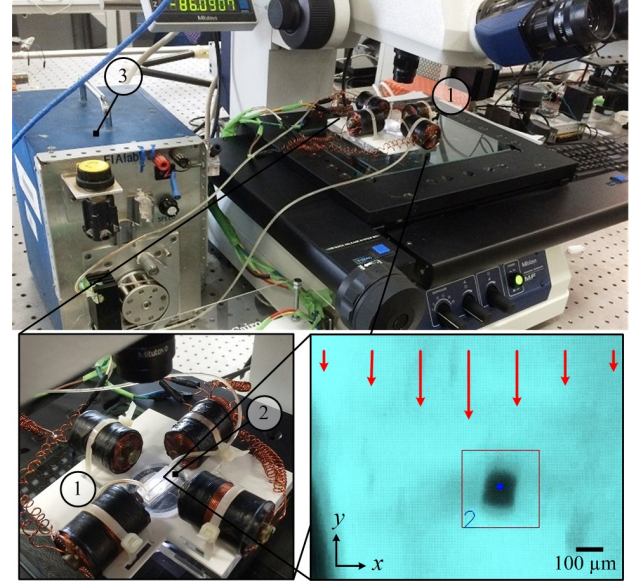


Figure 2. An electromagnetic system ① for the motion control of paramagnetic microparticles inside a fluidic channel ②. The inlet and outlet of the channel are connected to a dual pump (FIALab-3200 Dual Pump Sequential Injection Analyzer, FIALab Instruments Inc., Bellevue, USA). ③ to generate controlled time-varying flow rates. The inset shows that the magnetic field gradient holds a microparticle against a flow rate of 35 $\text{ml} \cdot \text{hr}^{-1}$. The reference position is indicated using the small blue circle. The red square indicates the position of the drug carrier and is assigned using our feature tracking algorithm. The red arrows indicate the direction of the flow. Please refer to the accompanying video that demonstrates a representative motion control of a paramagnetic microparticle against the flow of oil.

respectively. Since we can assume laminar flow, the drag force is given by the following Stokes' law:

$$\mathbf{F}_d(\dot{\mathbf{P}}) = 6\pi\eta r_p (\mathbf{v}(\mathbf{P}) - \dot{\mathbf{P}}), \quad (5)$$

where η is the dynamic viscosity of the fluid and r_p is the radius of the microparticle. $\dot{\mathbf{P}}$ and \mathbf{v} are the velocity vectors of the microparticle and the fluid with respect to a reference frame, respectively. The maximum drag force is observed when the microparticle moves against the flow along the positive y -axis, whereas minimum drag force occurs when the microparticle moves with the flow along the negative y -axis. We rewrite (1) using (2), (4) and (5) to obtain

$$\dot{\mathbf{P}} = \frac{\Lambda(\mathbf{m}, \mathbf{P}) \mathbf{I}}{6\pi\eta r_p} - \frac{2}{A} \left[\frac{M_p \dot{Q} \rho_f}{6\pi\eta r_p \rho_p} + Q \right] \left(1 - \frac{4x^2}{w^2}\right) \hat{\mathbf{y}}. \quad (6)$$

We study the motion control of paramagnetic microparticles inside a fluidic channel for the following cases: motion control in a stationary fluid, control against a unidirectional flow along a single axis, and motion control in the xy plane against unidirectional flows.

2.1 Motion of microparticles in a stationary fluid

In a stationary fluid, as shown in Fig. 3, $Q=0$ and $\dot{Q}=0$, (6) is given by

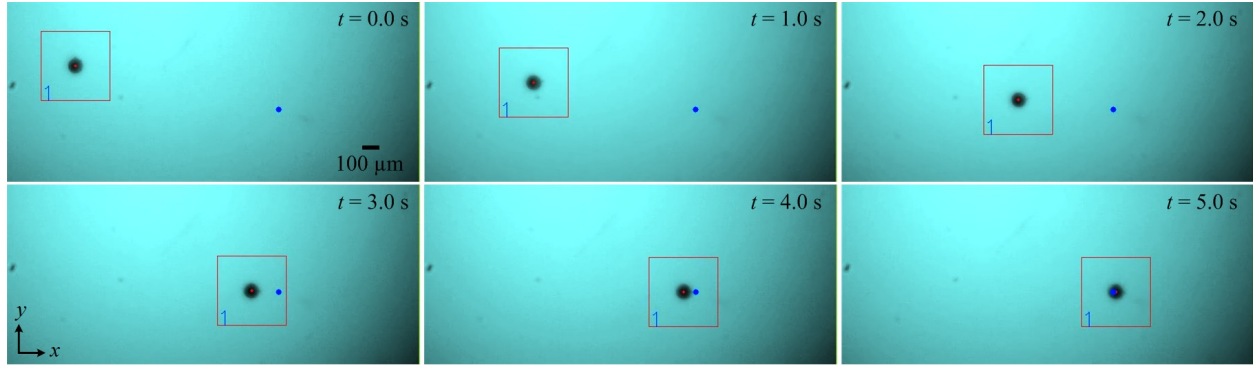


Figure 3. A representative closed-loop motion control of a paramagnetic microparticle in the absence of flow. The red square and the small blue circle indicate the position of the microparticle and the reference position, respectively, and are assigned using our feature tracking algorithm [35]. Please refer to the accompanying video that demonstrates the motion control of microparticles in a fluidic channel with zero flow.

$$\dot{\mathbf{P}} = \frac{\Lambda(\mathbf{m}, \mathbf{P})\mathbf{I}}{6\pi\eta r_p}. \quad (7)$$

The motion of the microparticle is controlled by the magnetic field gradient. Fig. 3 shows the motion of a microparticle under the influence of the magnetic field gradient in a stationary fluid. In this representative experiment, the microparticle is pulled at an average speed of $80 \mu\text{m}\cdot\text{s}^{-1}$ towards the reference position (small blue circle). Using (6), the magnetic force-current map entry ($\sqrt[3]{\sum \Lambda_{2i}^2}$) is calculated to be $1.3 \text{ nN}\cdot\text{A}^{-1}$, for current input of 3 A.

2.2. Motion of microparticles in a fluid with constant unidirectional flow along a single axis

A constant unidirectional flow rate ($\dot{Q}=0$) is generated inside a fluidic channel using a dual pump (FIALab-3200 Dual Pump Sequential Injection Analyzer, FIALab Instruments Inc., Bellevue, USA). This pump is connected to the inlet and outlet of the channel to provide controlled flow rates (Fig. 2). The microparticle is moved along the flow direction ($\hat{\mathbf{y}}$ - direction, x - constant). Therefore, the speed of the microparticle is given by

$$\dot{\mathbf{P}} = \left[\frac{\sum \Lambda_{2i} I_i}{6\pi\eta r_p} - \frac{2Q}{A} \left(1 - \frac{4x^2}{w^2} \right) \right] \hat{\mathbf{y}}. \quad (8)$$

The velocity ($\dot{\mathbf{P}}$) is plotted for constant currents (I_i), as shown in Fig. 4; parallel lines with slope of $-2 \left(1 - \frac{4x^2}{w^2} \right) / (A)$ are expected. If the microparticle moves at the centre-line of the channel ($x=0$), the slope reduces to $-\frac{2}{A}$. If the current is increased, the velocity increases. From the extension of the lines $\dot{\mathbf{P}}(Q)$ to the $\dot{\mathbf{P}}$ -axis and $\sum \Lambda_{2i} I_i / (6\pi\eta r_p)$, the magnetic moment of the magnetic microparticle is calculated. We implement this case experimentally for current inputs of 2.4 A, 3.5 A, and 4.7 A, as shown in Fig. 4. The average speed

of the paramagnetic microparticle is calculated for flow rates of $0 \text{ ml}\cdot\text{hr}^{-1}$ to $35 \text{ ml}\cdot\text{hr}^{-1}$. Our electromagnetic system cannot provide magnetic field gradient to overcome flow rates of more than $35 \text{ ml}\cdot\text{hr}^{-1}$. As expected, the graph shows approximately parallel lines. A slope of approximately -7200 m^{-2} indicates that the microparticle moves at $x=1.43 \text{ mm}$ away from the centre-line. The speed of the microparticle increases with the current in the magnetic coils during experiments and in the model, as described using (8). In the experiment, the speed at zero flow rate is $55 \mu\text{m}\cdot\text{s}^{-1}$, $105 \mu\text{m}\cdot\text{s}^{-1}$, and $135 \mu\text{m}\cdot\text{s}^{-1}$ for current (I_1) of 2.4 A, 3.5 A, and 4.7 A, respectively. Therefore, Λ_{21} is $1.1 \text{ nN}\cdot\text{A}^{-1}$, $1.4 \text{ nN}\cdot\text{A}^{-1}$, and $1.4 \text{ nN}\cdot\text{A}^{-1}$. With field gradients of $56 \text{ mT}\cdot\text{mm}^{-1}$, $122 \text{ mT}\cdot\text{mm}^{-1}$, and $221 \text{ mT}\cdot\text{mm}^{-1}$, the magnetic moment is calculated to be $19 \times 10^{-12} \text{ A}\cdot\text{m}^2$, $12 \times 10^{-12} \text{ A}\cdot\text{m}^2$, and $6 \times 10^{-12} \text{ A}\cdot\text{m}^2$. Hence, the average magnetic dipole moment of the microparticle is $12 \times 10^{-12} \text{ A}\cdot\text{m}^2$.

2.3. Motion of microparticles in a step-wise changing unidirectional flow along the xy plane

In this case, the flow is changed step-wise with N steps at times t_n as follows:

$$Q(t) = Q_0 + \sum_{n=1}^N H(t - t_n)(Q_n - Q_{n-1}), \quad (9)$$

where $H(\hat{t})$ is the Heaviside step function, which is zero for $\hat{t} < 0$ and one for $\hat{t} > 0$. Q_0 is the initial flow rate, and Q_n is the flow rates at times t_n . The derivative of H is the delta function $\delta(\hat{t})$ and is given by

$$\dot{Q}(t) = \sum_{n=1}^N \delta[t - t_n](Q_n - Q_{n-1}). \quad (10)$$

Therefore, the velocity ($\dot{\mathbf{P}}$) is only disturbed for an infinitesimally short time when the flow is changed. This effect can be seen in Fig. 5 where $\dot{\mathbf{P}}$ changes smoothly and control is achieved if the flow rate is changed. Motion along the

x -axis is achieved if the magnetic field gradient has an x component. This x component can be produced with the two coils perpendicular to the direction of the flow. In this case, the velocity of the microparticle is given by

$$\dot{\mathbf{P}} = \frac{\Lambda(\mathbf{m}, \mathbf{P})\mathbf{I}}{6\pi\eta r_p} - \frac{2Q}{A} \left(1 - \frac{4x^2}{w^2}\right) \hat{\mathbf{y}}. \quad (11)$$

The model of the microparticle is used in the design of a closed-loop motion control system inside a fluidic channel with time-varying flow rates.

3. Motion Control Inside Fluidic Channel with Time-varying Flow Rates

Motion control of microparticles inside a fluidic channel is achieved using a PD control system, PD control with disturbance compensation, and an optimal control system.

3.1 Design of proportional-derivative control system

The magnetic field gradients are controlled using (2) to pull the microparticle towards a reference position and achieve positioning within the vicinity of the reference position against different flow rates. For this, we devise a PD control system. Therefore, (1) can be rewritten as follows:

$$0 = \mathbf{K}_p \mathbf{e} + \mathbf{K}_d \dot{\mathbf{e}} + 6\pi\eta r_p \left(-\frac{Q}{A} \hat{\mathbf{y}} \pm \dot{\mathbf{P}}\right), \quad (12)$$

where $\mathbf{e} \in \mathbb{R}^{3 \times 1}$ and $\dot{\mathbf{e}} \in \mathbb{R}^{3 \times 1}$ are the position and velocity tracking errors, respectively. $\mathbf{K}_p \in \mathbb{R}^{3 \times 3}$ and $\mathbf{K}_d \in \mathbb{R}^{3 \times 3}$ are matrices of the proportional and derivative control gains, respectively [27]. In (12), the errors are calculated using [27]

$$\mathbf{e} = \mathbf{P} - \mathbf{P}_{\text{ref}} \quad \text{and} \quad \dot{\mathbf{e}} = \dot{\mathbf{P}}, \quad (13)$$

where $\mathbf{P}_{\text{ref}} \in \mathbb{R}^{3 \times 1}$ is a fixed reference position. Using (12) in (13), the error dynamics are calculated to be

$$\dot{\mathbf{e}} + (\mathbf{K}_d + \beta\mathbf{\Pi})^{-1} \mathbf{K}_p \mathbf{e} = \frac{\beta}{A} (\mathbf{K}_d + \beta\mathbf{\Pi})^{-1} Q \hat{\mathbf{y}}, \quad (14)$$

where $\mathbf{\Pi} \in \mathbb{R}^{3 \times 3}$ is the identity matrix and β is given by

$$\beta \triangleq 6\pi\eta r_p. \quad (15)$$

Fig. 3 shows a representative closed-loop motion control of a microparticle in a stationary fluid. The microparticle is pulled towards the reference position using the PD control input (first two terms in (12)). In this experiment, we observe that the microparticle is controlled at an average speed of $150 \mu\text{m.s}^{-1}$ and the steady-state error is $3 \mu\text{m}$. The error dynamics (12) indicate that the gain matrices must be positive-definite to achieve stable position control of the microparticle. In a stationary fluid ($\dot{Q}=0$) (Fig. 3), the last

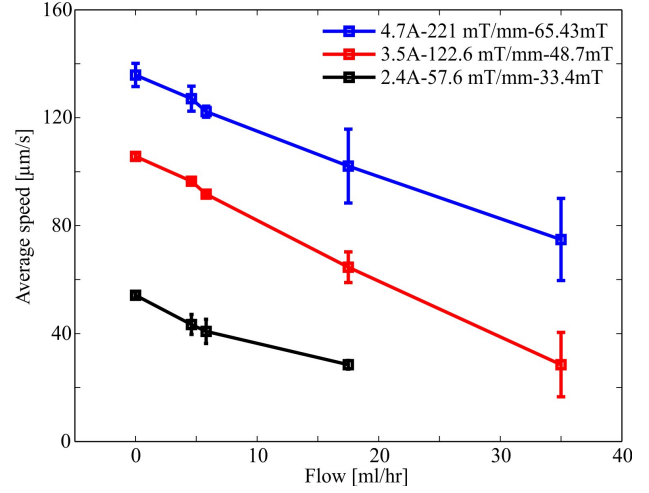


Figure 4. Characterization of the average speed of the paramagnetic microparticle against five representative flow rates. This experiment is repeated using three current inputs. Input current of 2.4 A (black line) provides magnetic field gradient of 56 mT.mm^{-1} and magnetic field of 33 mT . Input current of 3.5 A (red line) provides magnetic field gradient of 122 mT.mm^{-1} and magnetic field of 48 mT . Input current of 4.7 A (blue line) provides magnetic field gradient of 221 mT.mm^{-1} and magnetic field of 65 mT . The average speed is calculated using five open-loop trials along the y -axis using microparticles with average diameter of $100 \mu\text{m}$.

term in (12) is zero. Therefore, selecting \mathbf{K}_p and \mathbf{K}_d to be positive-definite achieves stable asymptotic stability of the microparticle. The control gains \mathbf{K}_p and \mathbf{K}_d are diagonal and have equal diagonal elements of 0.01 kg.s^{-2} and 0.015 kg.s^{-1} , respectively. In the presence of flow rate ($Q = \frac{dV}{dt}$), the right-hand side of (14) is not zero. Therefore, the closed-loop control characteristics are affected.

We apply flow rates of 4 ml.hr^{-1} , 6 ml.hr^{-1} , 17 ml.hr^{-1} , and 35 ml.hr^{-1} , and control the motion of the microparticle at each flow rate using similar control gains (12), as shown in Fig. 5. At flow rate of 4 ml.hr^{-1} , the speed of the microparticle against the flowing stream of the fluid is measured to be $150 \mu\text{m.s}^{-1}$, whereas the steady-state error is calculated to be $10 \mu\text{m}$. At flow rate of 35 ml.hr^{-1} , the average speed of the microparticle against the flow is decreased to $125 \mu\text{m.s}^{-1}$ and the steady-state error is increased to $64 \mu\text{m}$. Please refer to the accompanying video that demonstrates the closed-loop motion control of a microparticle against the four flow rates using the PD control system. The transient- and steady-state characteristics of the PD control system are affected by the varying flow rate. Therefore, this effect can be compensated using disturbance estimation and compensation.

3.2. Design of proportional-derivative control system with disturbance estimation and compensation

The drag force and the force due to time-varying flow rate exerted on the microparticle can be estimated using its velocity and the current inputs to the electromagnetic coils [22, 29, 30, 31, 32]. The estimated disturbance force ($\mathbf{d}(\dot{\mathbf{P}})$) is given by

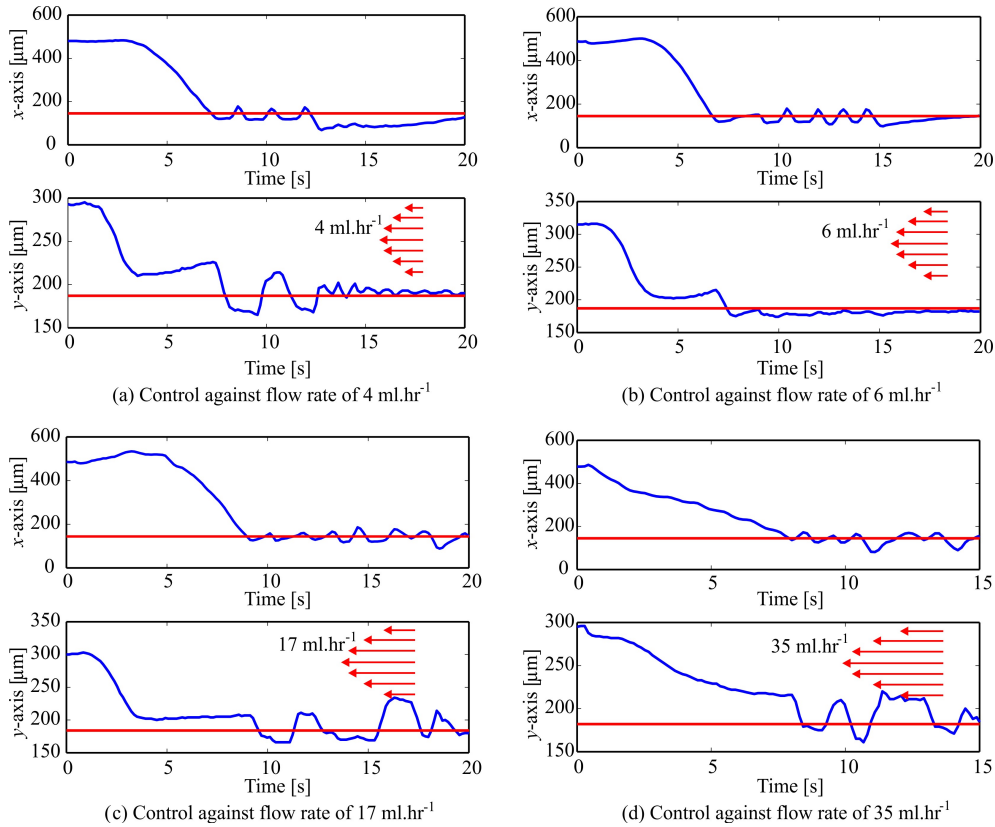


Figure 5. A representative motion control result of a microparticle against flow rates of 4 ml.hr⁻¹, 6 ml.hr⁻¹, 17 ml.hr⁻¹, and 35 ml.hr⁻¹ using control law (12). The control gains \mathbf{K}_p and \mathbf{K}_d are diagonal and have equal diagonal elements of 0.01 kg.s⁻² and 0.015 kg.s⁻¹, respectively. (a) At flow rate of 4 ml.hr⁻¹, the average speed and maximum steady-state error of the controlled particle are 150 $\mu\text{m.s}^{-1}$ and 10 μm , respectively. (b) At flow rate of 6 ml.hr⁻¹, the average speed and maximum steady-state error of the controlled particle are 145 $\mu\text{m.s}^{-1}$ and 47 μm , respectively. (c) At flow rate of 17 ml.hr⁻¹ the average speed and maximum steady-state error of the controlled particle are 135 $\mu\text{m.s}^{-1}$ and 55 μm , respectively. (d) At flow rate of 35 ml.hr⁻¹, the average speed and maximum steady-state error of the controlled particle are 125 $\mu\text{m.s}^{-1}$ and 64 μm , respectively. Please refer to the accompanying video that demonstrates the motion control of a microparticle against different flow rates using a PD control system.

$$\hat{\mathbf{d}}(\dot{\mathbf{P}}) = \frac{g}{s+g} (\mathbf{F}_n(\mathbf{P}) + gM_n\dot{\mathbf{P}}) - gM_n\dot{\mathbf{P}}, \quad (16)$$

where g is the gain of the low-pass filter, and $\mathbf{F}_n(\mathbf{P})$ is the nominal magnetic force exerted on the microparticle. Further, M_n is the nominal mass of the microparticle. Now, we devise a PD control system with disturbance compensation by adding the estimated disturbance to (12) as follows:

$$0 = -\hat{\mathbf{d}}(\dot{\mathbf{P}}) + \mathbf{K}_p\mathbf{e} + \mathbf{K}_d\dot{\mathbf{e}} + 6\pi\eta r_p \left(-\frac{Q}{A}\hat{\mathbf{y}} - \dot{\mathbf{P}} \right). \quad (17)$$

The first three terms in (17) represent the PD control input with disturbance compensation. The estimated disturbance force is a positive-feedback loop that allows for the compensation of the disturbance drag force in the channel, whereas the second and third terms provide the outer loop that stabilizes the motion of the microparticle [22].

Fig. 6 provides a representative motion control result of a microparticle against flow rates of 4 ml.hr⁻¹, 6 ml.hr⁻¹, 17 ml.hr⁻¹, and 35 ml.hr⁻¹. Control law (17) is implemented

with similar control gains for the mentioned flow rates. The control gains \mathbf{K}_p and \mathbf{K}_d are diagonal and have equal diagonal elements of 0.01 kg.s⁻² and 0.015 kg.s⁻¹, respectively; the gain (g) of the low-pass filter is selected to be 10 rad.s⁻¹. We observe that the disturbance estimation and compensation allows for improving the transient- and steady-state characteristics of the control system. At flow rate of 4 ml.hr⁻¹, the speed of the microparticle against the flowing stream of the fluid is measured to be 305 $\mu\text{m.s}^{-1}$, whereas the steady-state error is calculated to be 5 μm . At flow rate of 35 ml.hr⁻¹, the average speed of the particle against the flow is increased to 375 $\mu\text{m.s}^{-1}$ and the steady-state error is increased to 64 μm . Please refer to the accompanying video that demonstrates the closed-loop motion control of a microparticle against four flow rates using the PD control system with disturbance compensation.

The PD control system with disturbance compensation allows the microparticle to overcome time-varying flow rates, as shown in Fig. 7. In this experiment, the flow rate is increased from 6 ml.hr⁻¹ to 17 ml.hr⁻¹ at time $t=28$ seconds. At time $t=68$ seconds, the flow rate is increased from 17 ml.hr⁻¹ to 35 ml.hr⁻¹. The disturbance caused by the time-varying flow is compensated by the additional control

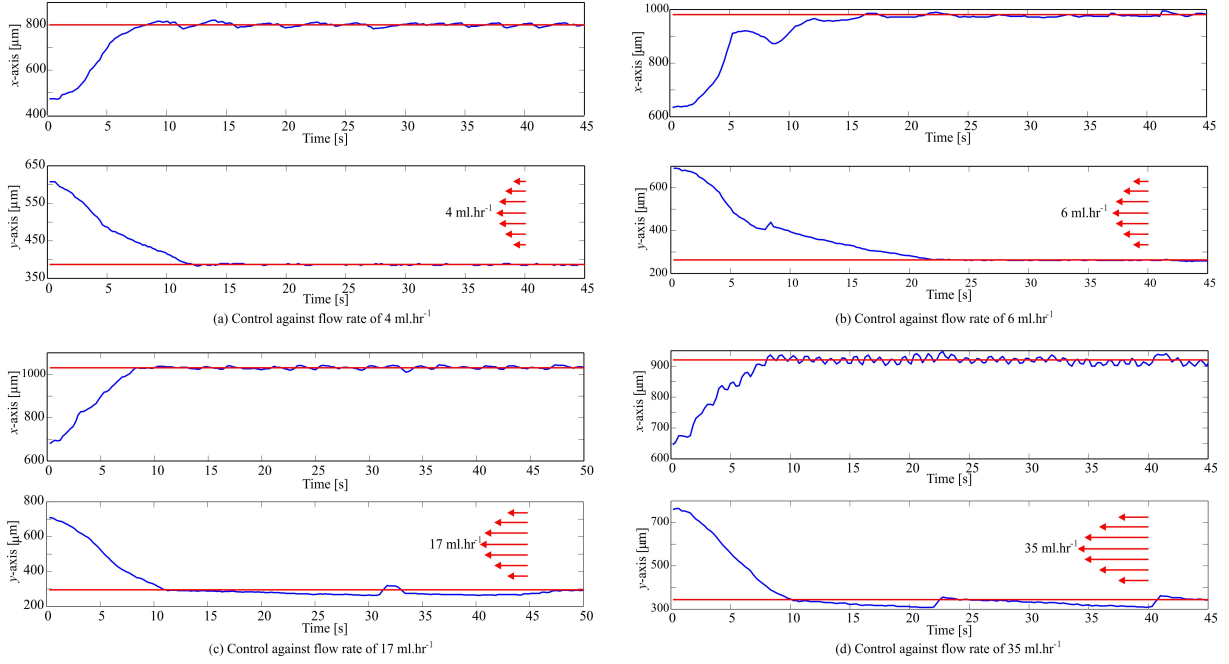


Figure 6. A representative motion control result of a microparticle against flow rates of 4 ml.hr⁻¹, 6 ml.hr⁻¹, 17 ml.hr⁻¹, and 35 ml.hr⁻¹ using control law (17). The control gains \mathbf{K}_p and \mathbf{K}_d are diagonal and have equal diagonal elements of 0.01 kg.s⁻² and 0.015 kg.s⁻¹, respectively; the gain (g) of the low-pass filter is 10 rad.s⁻¹. (a) At flow rate of 4 ml.hr⁻¹, the average speed and maximum steady-state error of the controlled particle are 300 $\mu\text{m.s}^{-1}$ and 5 μm , respectively. (b) At flow rate of 6 ml.hr⁻¹, the average speed and maximum steady-state error of the controlled particle are 322 $\mu\text{m.s}^{-1}$ and 14 μm , respectively. (c) At flow rate of 17 ml.hr⁻¹, the average speed and maximum steady-state error of the controlled particle are 350 $\mu\text{m.s}^{-1}$ and 15 μm , respectively. At flow rate of 35 ml.hr⁻¹, the average speed and maximum steady-state error of the controlled particle are 370 $\mu\text{m.s}^{-1}$ and 64 μm , respectively. Please refer to the accompanying video that demonstrates the motion control of a microparticle against different flow rates using a PD control system with disturbance compensation.

input ($\hat{\mathbf{d}}(\hat{\mathbf{P}})$). This compensation is demonstrated by the current input to the electromagnetic coils during the increase of the flow rates. The green line (Fig. 7) represents norm-2 ($\|\mathbf{I}\|_2$) of the input current vector. The control law (17) compensates for the time-varying flow through the estimation and addition of $\hat{\mathbf{d}}(\hat{\mathbf{P}})$. At flow rate of 6 ml.hr⁻¹, norm-2 is calculated to be 1.2 A in the steady state. Norm-2 of the current input is increased to 2 A and 3.4 A for flow rates of 17 ml.hr⁻¹ and 35 ml.hr⁻¹, respectively. Please refer to the accompanying video that demonstrates the closed-loop motion control of a microparticle against fluid with time-varying flow rate using the PD control system with disturbance compensation.

3.3 Design of optimal control system

An optimal path has to be determined to pull the microparticle against the flowing streams of a fluid while minimizing a cost function, such as the time to reach a reference position, the input current vector, or the total energy [21]. We assume that the microparticle moves from the point $\mathbf{P}_i=(x_{0r}, y_{0r}, z_{0r})$ to the point $\mathbf{P}_f=(x_f, y_f, z_f)$ in a fixed time T , as shown in Fig. 1. We devise the following cost function ($J(\mathbf{P}(t))$):

$$J(\mathbf{P}(t)) = \int_0^T \dot{\mathbf{P}}^T \dot{\mathbf{P}} dt. \quad (18)$$

Therefore, the Hamiltonian function ($\mathcal{H}(\mathbf{P}, \mathbf{I}, \lambda, t)$) is given by [33, 34]

$$\mathcal{H} = \dot{\mathbf{P}}^T \dot{\mathbf{P}} - \mathbf{P}^T \mathbf{P} + \lambda \left(\mathbf{\Lambda}(\mathbf{m}, \mathbf{P}) \mathbf{I} + \beta \left(\dot{\mathbf{P}} - \frac{\dot{Q}}{A} \hat{\mathbf{x}} \right) \right), \quad (19)$$

where λ is a vector of the co-states. The necessary condition on the optimal path is given by [33]

$$\dot{\mathbf{P}}^* = \frac{\partial \mathcal{H}}{\partial \lambda}(\mathbf{P}^*, \mathbf{I}^*, \lambda^*, t), \quad (20)$$

where $\dot{\mathbf{P}}^*$ is the time-derivative of the optimal path of the microparticle. The optimal co-states are given by

$$\dot{\lambda}^* = \frac{\partial \mathcal{H}}{\partial \mathbf{P}}(\mathbf{P}^*, \mathbf{I}^*, \lambda^*, t), \quad (21)$$

where λ^* is a vector of the optimal co-states. Finally, the optimal current input (\mathbf{I}^*) is given using

$$0 = \frac{\partial \mathcal{H}}{\partial \mathbf{I}}(\mathbf{P}^*, \mathbf{I}^*, \lambda^*, t). \quad (22)$$

Equations (20), (21), and (22) are solved simultaneously for the optimal path (\mathbf{P}^*), optimal co-states (λ^*), and optimal

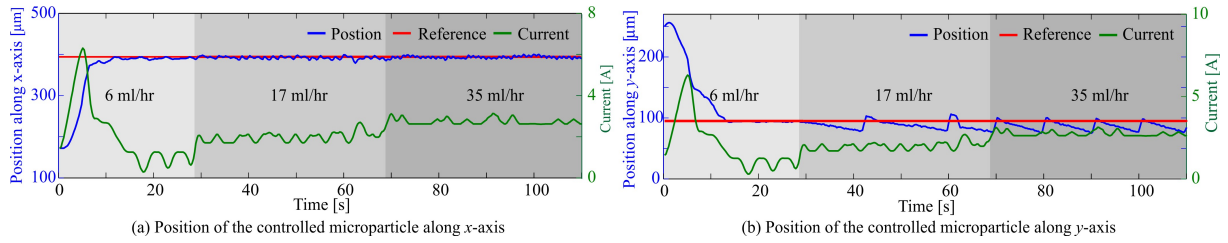


Figure 7. A representative closed-loop motion control of a paramagnetic microparticle against fluid with time-varying flow rate. The flow rate is increased at time $t = 28$ seconds and $t = 68$ seconds to 17 ml.hr^{-1} and 35 ml.hr^{-1} , respectively. The green line indicates norm-2 of the current vector to show the effect of the compensating control input. This input mitigates the effect of the time-varying flow and allows the microparticle to be localized within the vicinity of the fixed reference position (indicated by the red line). The control gains \mathbf{K}_p and \mathbf{K}_d are diagonal and have equal diagonal elements of 0.01 kg.s^{-2} and 0.015 kg.s^{-1} , respectively; the gain (g) of the low-pass filter is 10 rad.s^{-1} . (a) Position of the controlled microparticle on the x -axis. (b) Position of the controlled microparticle on the y -axis. Please refer to the accompanying video that demonstrates the closed-loop motion control of a microparticle against fluid with time-varying flow rate using the PD control system with disturbance compensation.

current input (\mathbf{I}^*). We obtain the following optimal path for the microparticle:

$$x^* = \frac{1}{1-\beta} \left(\frac{y^{*2}}{w^2} - v_{\max} \right), \quad (23)$$

where w is the width of the fluidic channel and v_{\max} is the maximum flow in the middle of the channel. x^* and y^* are the components of the optimal path of the microparticle. Equation (23) is a necessary condition for the optimal path that minimizes the kinetic energy function ($\mathbf{P}^T \mathbf{P}$) of the microparticle. This equation indicates that a quadratic path has to be followed to minimize the energy of the microparticle against the flow inside the fluidic channel. Fig. 1 shows the optimal path between two points along the channel, (\mathbf{P}_i and \mathbf{P}_f). The quadratic path allows the microparticle to avoid maximum force due to flow (2). The microparticle moves towards the wall of the channel to minimize the drag and flow forces exerted on its surface, and hence reaches the reference position with minimal energy.

Our control system assigns waypoints along the optimal path (small orange points), and the microparticle is pulled towards each of the waypoints, as shown in Fig. 8. In this representative experiment, the microparticle is controlled at an average speed of $386 \mu\text{m.s}^{-1}$ and is localized at the reference position with maximum error of $5 \mu\text{m}$. The initial position of the microparticle and the reference position (small blue circle) are adjusted to be aligned along the centre-line of the fluidic channel. This adjustment subjects the microparticle to maximum flow (v_{\max}). The maximum flow rate, the width of the channel, and the constant (β) of the microparticle and magnetic system are used to calculate the optimal path using (23). We repeat this experiment at flow rates of 4 ml.hr^{-1} , 6 ml.hr^{-1} , 17 ml.hr^{-1} , and 35 ml.hr^{-1} , as shown in Fig. 9. The optimal path is calculated at each time, and waypoints are provided for the optimal control system to pull the microparticles towards the reference position (vertical red line). The average speeds of the microparticle are calculated to be 350.18

$\mu\text{m.s}^{-1}$, $442.63 \mu\text{m.s}^{-1}$, $468.86 \mu\text{m.s}^{-1}$, and $557.4 \mu\text{m.s}^{-1}$ for flow rates of 4 ml.hr^{-1} , 6 ml.hr^{-1} , 17 ml.hr^{-1} , and 35 ml.hr^{-1} , respectively. The maximum position errors in the steady state are calculated to be $10 \mu\text{m}$, $10 \mu\text{m}$, $15 \mu\text{m}$, and $16 \mu\text{m}$ for flow rates of 4 ml.hr^{-1} , 6 ml.hr^{-1} , 17 ml.hr^{-1} , and 35 ml.hr^{-1} , respectively. Please refer to the accompanying video that demonstrates the optimal control of microparticles against time-varying flow rates.

Table 1 provides a comparison between the PD control system, PD control with disturbance compensation, and optimal control system in the transient (rise time and average speed) and steady state (maximum position error). The rise time (time taken by the microparticle to reach the reference position) of the optimal control system is greater than that of the PD control system and the PD control system with disturbance compensation. The optimal control system pulls the microparticle along the optimal path, as shown in Fig. 8. Therefore, the microparticle does not move along the shortest path and the rise time is increased compared to the PD control system. Nevertheless, we observe from the comparison in Table 1 that the microparticle reaches maximum speed under the influence of the optimal control system for all flow rates. We attribute this increase in the average speed to the optimal path taken by the controlled microparticle. This optimal path is quadratic (based on (23)) and allows the microparticle to avoid maximum forces due to drag and time-varying flow. The microparticle moves towards the walls of the fluidic channel where the flow is lower than that at the middle of the channel based on (3). The PD control system does not provide an optimal trajectory for the microparticle, but it does provide a magnetic force pulling towards the reference position regardless of the direction of flow, initial position of the microparticle, and reference position. Therefore, the microparticle is subjected to maximum force due to the time-varying flow in the channel.

4. Discussions

The magnetic-based control systems presented in this study are fairly general, even though the experimental work is done using paramagnetic microparticles of spher-

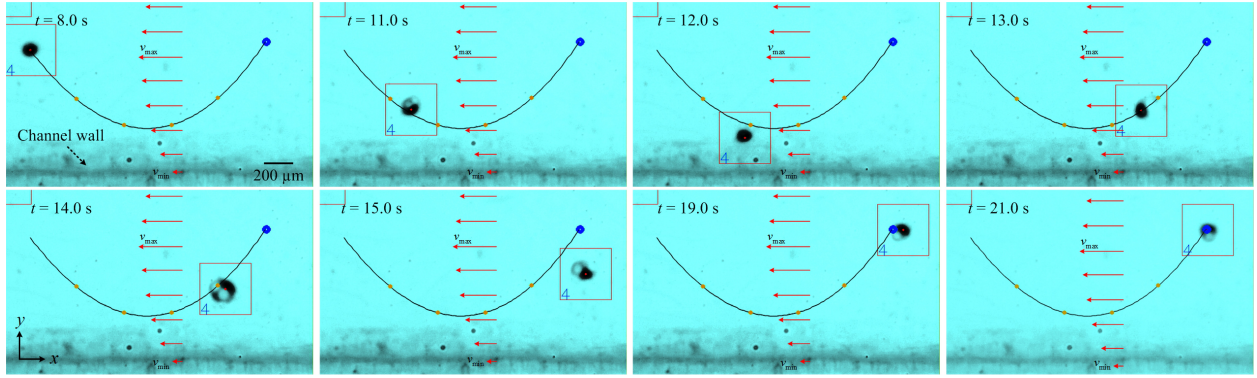


Figure 8. A representative motion control along an optimal path (black curve) between the initial (at $t=8.0$ seconds) and reference position (small blue circle) of the microparticle. The orange points indicate waypoints that are assigned by our closed-loop control system along the optimal path. The optimal path is calculated using (23) and the microparticle is pulled towards the waypoints using the optimal input (22). The flow rate in this experiment is 35 ml.hr^{-1} . The horizontal dark line indicates the edge of the fluidic channel. The dashed black arrows indicate the walls of the channel. Please refer to the accompanying video that demonstrates our motion control along an optimal path.

ical geometry. These control systems can be implemented on microrobots such as artificial helical flagella [38, 39], magnetotactic bacteria, superparamagnetic particles, ferromagnetic particles, and microparticles with irregular shapes. The range of flow rates used in this study is similar to that used in animal experimentation. Mouse carotid flow rates average approximately between 14.4 ml.hr^{-1} and 42 ml.hr^{-1} [20]. Therefore, the electromagnetic configuration and the magnetic-based control system hold promise for medical application. They allow us to navigate microparticles controllably against flow rates that are similar to those used in animal experimentation. Therefore, they can be used to implement targeted drug delivery using mice or test chemotherapeutic agents coated on the microparticles *in vivo*. However, the following challenges still need to be addressed in order to translate the targeted drug delivery using magnetic microparticles into *in vivo* experimentation:

- The flow rates of blood in the aorta, arteries, capillaries, veins, and vena cava are higher than the flow rates used in this study and necessitate larger magnetic field gradient to move and hold the microparticles;
- Clinical imaging modality must be integrated into the electromagnetic configuration to provide feedback to the control system, and its resolution has to be at the micro scale;
- The biocompatibility and physiological conditions of the drug release must be studied and implemented experimentally.

The closed configuration of electromagnetic coils cannot be scaled up to the scale of *in vivo* devices. Therefore, the first challenge can be overcome using an electromagnetic system with open configuration [40, 41]. The second challenge can also be overcome using an electromagnetic system with open configuration, since it will provide larger space to incorporate an imaging modality, e.g., an ultrasound system [36]. The ultrasound probe can be moved using a robotic arm in relation to a permanent magnet that is fixed to the end-effector of another robotic arm. This

configuration will enable motion control and positioning of magnetic drug carriers throughout relatively large workspaces and with higher field gradient than that provided by electromagnetic systems with closed configurations. The biocompatibility of the used microparticles and the amounts of drug required for the therapy should be optimized; the drug release per unit time should also be taken into consideration based on the binding and rebinding between the targeted drug and the microparticles they are immobilized on. This should be optimized first *in vitro* under similar experimental conditions to the physiological ones in terms of the amount of drug to be immobilized, pH, matrix, and flow rate.

5. Conclusions and Future Work

This paper has reported an experimental demonstration of motion control of paramagnetic microparticles against flowing streams of a fluid using a PD control system with and without disturbance compensation. The PD control allows a controlled microparticle to move against flow of 35 ml.hr^{-1} at average speed of $125 \mu\text{m.s}^{-1}$, whereas the disturbance compensation achieves average speed of $375 \mu\text{m.s}^{-1}$. In the steady state, the PD control systems with and without disturbance compensation achieve positioning with maximum positioning error of $64 \mu\text{m}$ and $18 \mu\text{m}$, respectively, against flow of 35 ml.hr^{-1} . The robustness of the PD control with disturbance compensation is tested experimentally by applying time-varying flow rate of 14 ml.hr^{-1} to 35 ml.hr^{-1} . The additional disturbance control input compensates for the increased drag force and force due to time-varying flow rate, and achieves maximum position tracking error of $18 \mu\text{m}$ at flow rate of 25 ml.hr^{-1} . The optimal path between two points inside a fluidic channel has also been studied, using calculus of variation. We find that following a quadratic trajectory from the initial position to the final destination against the flow not only increases the speed of the microparticles (for all flow rates), but also achieves acceptable maximum position error compared to the PD control system with disturbance compensation.

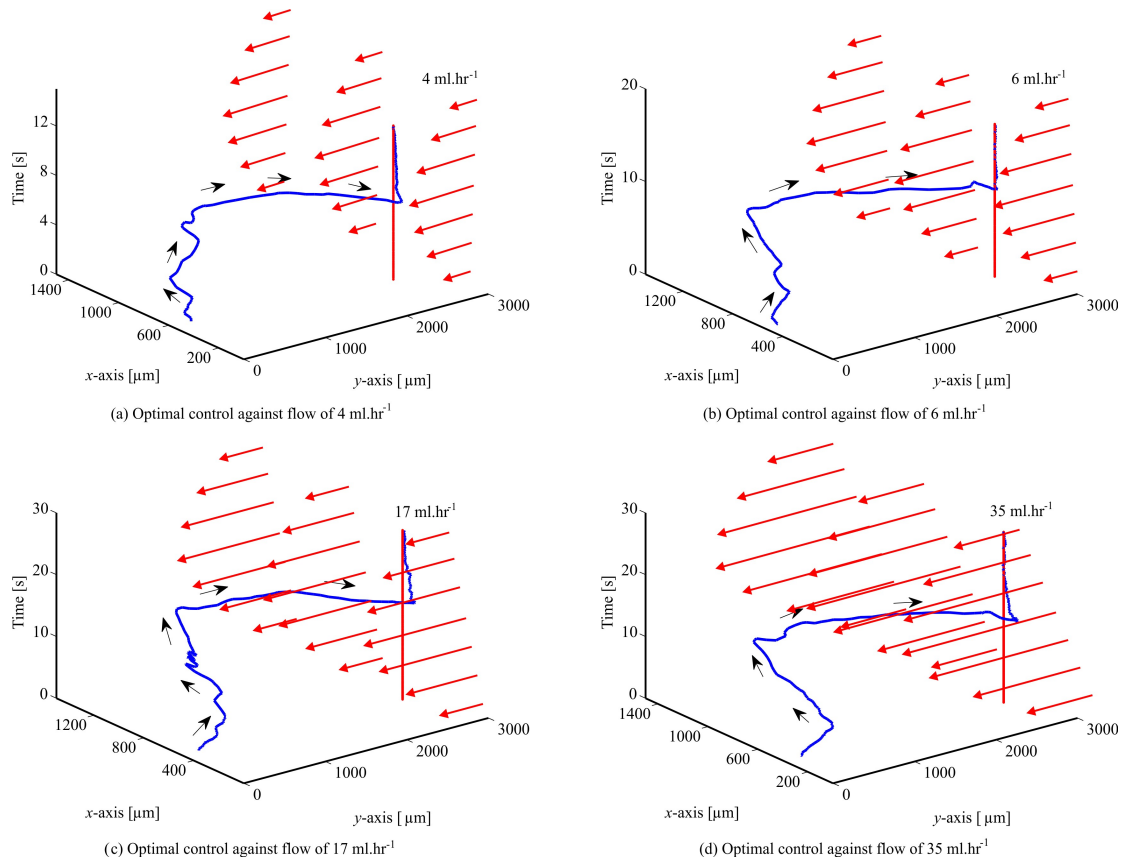


Figure 9. Optimal motion control of paramagnetic microparticles along an optimal trajectory between the initial position of the microparticle and the reference position. The flow is applied along the y -axis and the initial and reference positions are collinear with the maximum flow within the channel. The controlled microparticle follows a quadratic path (23) towards the reference position (vertical red line) against flow rates of 4 ml.hr^{-1} , 6 ml.hr^{-1} , 17 ml.hr^{-1} , and 35 ml.hr^{-1} . The black and red arrows indicate the direction of the microparticle and flow, respectively. (a, b, c, and d) Motion of the microparticle against flow rates of 4 ml.hr^{-1} , 6 ml.hr^{-1} , 17 ml.hr^{-1} , and 35 ml.hr^{-1} , respectively. Please refer to the accompanying video that demonstrates our motion control along an optimal path.

Flow Rate [ml.hr^{-1}]	Criterion	PD	PD with Compensation	Optimal Control
0	Average rise time [s]	2.8 ± 0.4	2.3 ± 0.8	10 ± 1.5
	Average speed [$\mu\text{m.s}^{-1}$]	150 ± 4.4	305 ± 4	298 ± 4
	Maximum error [μm]	2	2	3
4	Average rise time [s]	3.1 ± 0.5	3.1 ± 0.6	13.7 ± 9.9
	Average speed [$\mu\text{m.s}^{-1}$]	150 ± 4.4	305 ± 5.4	350.2 ± 15
	Maximum error [μm]	10	5	10
6	Average rise time [s]	6.6 ± 1.4	7.1 ± 0.2	9.9 ± 1.9
	Average speed [$\mu\text{m.s}^{-1}$]	145 ± 0.8	322 ± 0.7	442.6 ± 10
	Maximum error [μm]	47	14	10
17	Average rise time [s]	8.5 ± 0.4	5.7 ± 2	11.7 ± 3.5
	Average speed [$\mu\text{m.s}^{-1}$]	135 ± 4.6	350 ± 3.5	468.9 ± 3
	Maximum error [μm]	55	15	15
35	Average rise time [s]	20.1 ± 2.8	5.2 ± 0.3	12.75 ± 1.4
	Average speed [$\mu\text{m.s}^{-1}$]	125 ± 4.9	375 ± 3.4	557.4 ± 8
	Maximum error [μm]	64	18	16

Table 1. Closed-loop control characteristics of the proportional-derivative (PD) control system, PD control system with disturbance compensation, and optimal control system. The average rise time, average speed, and maximum error are calculated from 15 motion control trials at each flow rate. Control laws (12) and (17) are used to implement the PD control with and without disturbance compensation, respectively. The optimal path and optimal control input are calculated using (23) and (22), respectively.

In future studies, the motion control presented in this paper will be implemented in simulated body fluid, and our electromagnetic system will be adapted to incorporate a clinical imaging modality [36, 37]. In addition, the electromagnetic coils will be modified to generate magnetic field gradient larger than $220 \text{ mT}\cdot\text{m}^{-1}$ to enable the control of microparticles against flow rates greater than $35 \text{ ml}\cdot\text{hr}^{-1}$. We will also develop fluidic channels with multiple inlets to induce flow from arbitrary directions. This modification will enable us to study the robustness of the motion control system against arbitrary disturbance forces. The microparticles will be coated with chemotherapeutic agents and the physiological conditions of the drug release will be studied in the presence of time-varying flow.

6. Acknowledgements

The authors acknowledge the funding provided by the German University in Cairo and the DAAD-BMBF funding project. The authors also acknowledge the funding from the American University in Cairo (Faculty Support Research Grant).

The authors would like to thank Ms Heba Hassan for her assistance with the design of the optimal motion control system and for her valuable feedback during the preparation of this work.

7. References

- [1] Q. A. Pankhurst, J. Connolly, S. K. Jones, and J. Dobson, "Applications of magnetic nanoparticles in biomedicine," *Journal of Physics*, vol. 36, no. 13, pp. 167-181, June 2003.
- [2] B. J. Nelson, I. K. Kaliakatsos, and J. J. Abbott, "Microrobots for minimally invasive medicine," *Annual Review of Biomedical Engineering*, vol. 12, pp. 55-85, April 2010.
- [3] R. Sinha, G. J. Kim, S. Nie, and D. M. Shin, "Nanotechnology in cancer therapeutics: bioconjugated nanoparticles for drug delivery," *Molecular Cancer Therapeutics*, vol. 5, no. 8, pp. 1909-1917, August 2006.
- [4] S. Martel, O. Felfoul, J.-B. Mathieu, A. Chanu, S. Tamaz, M. Mohammadi, M. Mankiewicz, and N. Tabatabaei, "MRI-based medical nanorobotic platform for the control of magnetic nanoparticles and flagellated bacteria for target interventions in human capillaries," *The International Journal of Robotics Research*, vol. 28, no. 9, pp. 1169-1182, September 2009.
- [5] I. S. M. Khalil, I. E. O. Goma, R. M. Abdel-Kader and S. Misra, "Magnetic-Based contact and non-contact manipulation of cell mockups and MCF-7 human breast cancer cells," *Smart Drug Delivery System*, pp. 219-235, February 2016.
- [6] K. Belharet, D. Folio, and A. Ferreira, "Simulation and planning of a magnetically actuated microrobot navigating in the arteries," *IEEE Transactions on Biomedical Engineering*, vol. 60, no. 4, pp. 994-1001, April 2013.
- [7] B. J. Nelson, I. K. Kaliakatsos, and J. J. Abbott, "Microrobots for minimally invasive medicine," *Annual Review of Biomedical Engineering*, vol. 12, pp. 55-85, April 2010.
- [8] J. Wang and W. Gao, "Nano/Microscale Motors: Biomedical Opportunities and Challenges," *ACS Nano*, vol. 6, no. 7, pp. 5745-5751, July 2012.
- [9] K. Youakim, M. Ehab, O. Hatem, S. Misra and I. S. M. Khalil, "Paramagnetic microparticles sliding on a surface: characterization and closed-loop motion control," in *Proceedings of the IEEE International Conference on Robotics and Automation (ICRA)*, pp. 4068-4073, Seattle, Washington, USA, May 2015.
- [10] S. S. Shevkoplyas, A. C. Siegel, R. M. Westervelt, M. G. Prentiss, and G. M. Whitesides, "The force acting on a superparamagnetic bead due to an applied magnetic field," *Royal Society of Chemistry*, vol. 7, no. 6, pp. 1294-1302, July 2007.
- [11] J. Weizenecker, B. Gleich, J. Rahmer, H. Dahnke, and J. Borgert, "Three-dimensional real-time *in vivo* magnetic particle imaging," *Physics in Medicine and Biology*, vol. 54, no. 5, pp. 1-10, March 2009.
- [12] A. S. Lübbe, C. Bergemann, J. Brock, and D. G. McClure, "Physiological aspects in magnetic drug-targeting," *Journal of Magnetism and Magnetic Materials*, vol. 194, no. 1-3, pp. 149-155, April 1999.
- [13] S. R. Rudge, T. L. Kurtz, C. R. Vessely, L. G. Catterall, and D. L. Williamson, "Preparation, characterization, and performance of magnetic iron-carbon composite microparticles for chemotherapy," *Biomaterials*, vol. 21, no. 14, pp. 1411-1420, July 2000.
- [14] C. Alexiou, W. Arnold, R. J. Klein, F. G. Parak, P. Hulin, C. Bergemann, W. Erhardt, S. Wagenpfeil, and A. S. Lübbe, "Locoregional cancer treatment with magnetic drug targeting," *Cancer Research*, vol. 60, pp. 6641-6648, December 2000.
- [15] S. Sanchez, A. A. Solovev, S. M. Harazim, and O. G. Schmidt, "Microrobots swimming in the flowing streams of microfluidic channels," *Journal of the American Chemical Society*, vol. 133, no. 4, pp. 701-703, December 2010.
- [16] I. S. M. Khalil, M. P. Pichel, O. S. Sukas, L. Abelman, and S. Misra, "Control of magnetotactic bacterium in a micro-fabricated maze," in *Proceedings of the IEEE International Conference on Robotics and Automation (ICRA)*, pp. 5488-5493, Karlsruhe, Germany, May 2013.
- [17] I. S. M. Khalil, V. Magdanz, S. Sanchez, O. G. Schmidt and S. Misra, "Precise localization and control of catalytic janus micromotors using weak magnetic fields," *International Journal of Advanced Robotic Systems*, vol. 12, no. 2, pp. 1-7, June 2014.

- [18] K. Belharet, D. Folio, and A. Ferreira "Control of a magnetic microrobot navigating in microfluidic arterial bifurcations through pulsatile and viscous flow," in *Proceedings of the IEEE International Conference of Robotics and Systems (IROS)*, pp. 2559-2564, Vilamoura, Algarve, Portugal, October 2012.
- [19] I. S. M. Khalil, V. Magdanz, S. Sanchez, O. G. Schmidt, and S. Misra, "The control of self-propelled microjets inside a microchannel with time-varying flow rates," *IEEE Transactions on Robotics*, vol. 30, no. 1, pp. 49-58, February 2013.
- [20] A. Nacev, C. Beni, O. Bruno, and B. Shapiro, "Magnetic nanoparticle transport within flowing blood and into surrounding tissue," *Nanomed.*, vol. 5, no. 9, pp. 1459-1466, November 2010.
- [21] I. S. M. Khalil, R. M. P. Metz, B. A. Reefman, and S. Misra, "Magnetic-Based minimum input motion control of paramagnetic microparticles in three-dimensional space," in *Proceedings of the IEEE/RSJ International Conference of Robotics and Systems (IROS)*, pp. 2053-2058, Tokyo, Japan, November 2013.
- [22] I. S. M. Khalil, L. Abelmann, and S. Misra, "Magnetic-based motion control of paramagnetic microparticles with disturbance compensation," *IEEE Transactions on Magnetics*, vol. 50, no. 10 (5400110), October 2010.
- [23] M. Serry, A. Rubin, M. Ibrahim, and S. Sedky, "Silicon Germanium as a novel mask for silicon deep reactive ion etching," *Journal of Microelectromechanical Systems*, vol. 22, no. 5, pp. 1081-1088, October 2013.
- [24] M. P. Kummer, J. J. Abbott, B. E. Kartochovil, R. Borer, A. Sengul, and B. J. Nelson, "OctoMag: an electromagnetic system for 5-DOF wireless micro-manipulation," *IEEE Transactions on Robotics*, vol. 26, no. 6, pp. 1006-1017, December 2010.
- [25] T. H. Boyer, "The force on a magnetic dipole," *American Journal of Physics*, vol. 56, no. 8, pp. 688-692, August 1988.
- [26] B. R. Munson, W. W. Huebsch, and A. P. Rothmayer, "Fundamentals of fluid mechanics," Wiley, 2005.
- [27] I. S. M. Khalil, M. P. Pichel, L. Abelmann, and S. Misra, "Closed-loop control of magnetotactic bacteria," *The International Journal of Robotics Research*, vol. 32, no. 6, pp. 637-649, May 2013.
- [28] B. Esteban, J.-R. Riba, G. Baquero, A. Rius, and R. Puig, "Temperature dependence of density and viscosity of vegetable oils," *Biomass and bioenergy*, vol. 42, pp. 164-171, July 2012.
- [29] Z. J. Yang, H. Tsubakihara, S. Kanae, K. Wada, and C. Yi. Su, "A novel robust nonlinear motion controller with disturbance observer," *IEEE Transactions on Control Systems Technology*, vol. 16, no. 1, pp. 137-147, January 2008.
- [30] I. S. M. Khalil, A. Sabanovic, S. Misra, "An energy-based state observer for dynamical subsystems with inaccessible state variables", in *Proceedings of the IEEE International Conference of Robotics and Systems (IROS)*, pp. 3734-3740, Vilamoura, Algarve, Portugal, October 2012.
- [31] Y. Choi, K. Yang, W. K. Chung, H. R. Kim, and I. H. Suh, "On the robustness and performance of disturbance observers for second-order systems," *IEEE Transactions on Automatic Control*, vol. 48, no. 2, pp. 315-320, February 2003.
- [32] S. Katsura, Y. Matsumoto, and K. Ohnishi, "Modeling of force sensing and validation of disturbance observer for force control," *IEEE Transactions on Industrial Electronics*, vol. 54, no. 1, pp. 530-538, February 2007.
- [33] M. Athans and P. L. Falb, "Optimal control: An introduction to the theory and its applications," McGraw-Hill, New York, 1966.
- [34] D. E. Kirk, "Optimal control theory: an introduction," Dover Publications, Inc., Mineola, New York, 2004.
- [35] I. S. M. Khalil, K. Youakim, A. Sánchez, S. Misra "Magnetic-based motion control of sperm-shaped microrobots using weak oscillating magnetic fields," in *Proceedings of the IEEE International Conference of Robotics and Systems (IROS)*, pp. 4686-4691, September 2014.
- [36] I. S. M. Khalil, P. Ferreira, R. Eleutério, C. L. de Korte, and S. Misra, "Magnetic-based closed-loop control of paramagnetic microparticles using ultrasound feedback," in *Proceedings of the IEEE International Conference on Robotics and Automation (ICRA)*, pp. 3807-3812, Hong Kong, China, June 2014.
- [37] S. Martel, O. Felfoul, J.-B. Mathieu, A. Chanu, S. Tamaz, M. Mohammadi, M. Mankiewicz, and N. Tabatabaei, "MRI-based medical nanorobotic platform for the control of magnetic nanoparticles and flagellated bacteria for target interventions in human capillaries," *International Journal of Robotics Research*, vol. 28, no. 9, pp. 1169-1182, September 2009.
- [38] K. E. Peyer, L. Zhang, and B. J. Nelson, "Bio-inspired magnetic swimming microrobots for biomedical applications," *Nanoscale*, vol. 5, no. 4, pp. 1259-1272, November 2012.
- [39] D. J. Bell, S. Leutenegger, K. M. Hammar, L. X. Dong, and B. J. Nelson, "Flagella-like propulsion for microrobots using a magnetic nanocoil and a rotating electromagnetic field," in *Proceedings of the IEEE International Conference on Robotics and Automation (ICRA)*, pp. 1128-1133, April 2007.
- [40] A. W. Mahoney, J. C. Sarrazin, E. Bamberg, and J. J. Abbott, "Velocity control with gravity compensation for magnetic helical microswimmers," *Ad-*

- vanced Robotics*, vol. 28, no. 8, pp. 1007-1028, April 2012.
- [41] T. W. R. Fountain, P. V. Kailat, and J. J. Abbott, "Wireless control of magnetic helical microrobots using a rotating-permanent-magnet manipulator," in *Proceedings of the IEEE International Conference on Robotics and Automation (ICRA)*, pp. 576-581, Alaska, USA, May 2010.